Computational Study of Competition between Direct Abstraction and Addition-Elimination in the Reaction of Cl Atoms with Propene

Balázs Hornung,[1] Thomas J. Preston,[1] Shubhrangshu Pandit,[1] Jeremy N. Harvey[2] and Andrew J. Orr-Ewing[1*]

[1] School of Chemistry, University of Bristol, Cantock's Close, Bristol, BS8 1TS, United Kingdom.

[2] Department of Chemistry, KU Leuven, Celestijnenlaan 200F, B-3001 Leuven (Heverlee), Belgium.

19 August 2015

Keywords: quasi-classical trajectory; potential energy surface; empirical valence bond; alkene; radical.

Abstract

Quasi-classical trajectory calculations on a newly constructed and full-dimensionality potential energy surface (PES) examine the dynamics of the reaction of Cl atoms with propene. The PES is an empirical valence bond (EVB) fit to high-level *ab initio* energies and incorporates deep potential energy wells for the 1-chloropropyl and 2-chloropropyl radicals, a direct H-atom abstraction route to HCl + allyl radical (CH_2CHCH_2·) products ($\Delta_r H^{\ominus}_{298K}$ = −63.1 kJ mol^{-1}), and a pathway connecting these regions. In total, 94000 successful reactive trajectories were used to compute distributions of angular scattering and HCl vibrational and rotational level populations. These measures of the reaction dynamics agree satisfactorily with available experimental data. The dominant reaction pathway is direct abstraction of a hydrogen atom from the methyl group of propene occurring in under 500 fs. Fewer than 10% of trajectories follow an addition-elimination route *via* the two isomeric chloropropyl radicals. Large amplitude motions of the Cl about the propene molecular framework couple the addition intermediates to the direct abstraction pathway. The EVB method provides a good description of the complicated PES for the Cl + propene reaction despite fitting to a limited number of *ab initio* points, with the further advantage that dynamics specific to certain mechanisms can be studied in isolation by switching off coupling terms in the EVB matrix connecting different regions of the PES.

1. Introduction

Biogenic and anthropogenic sources emit a variety of saturated and unsaturated hydrocarbons into the Earth's troposphere.[1-2] In the marine boundary layer and polluted coastal areas, chlorine atom reactions with these volatile organic compounds (VOCs) compete with their removal by oxidation reactions with hydroxyl (OH) radicals.[3] Hydrogen-atom abstraction reactions produce alkyl or alkenyl radicals that react further with O_2; in the case of biogenic emissions of terpenes, the resulting enols and enones are potential contributors to secondary organic aerosol.[1]

Propene serves as a model for reactions of abundant atmospheric alkenes such as isoprene and higher terpenes because it contains both sp^2 (C=C) and sp^3 ($-CH_3$) hybridized carbon functionality. The gas-phase reaction of a chlorine atom with propene

$$Cl + CH_3CHCH_2 \rightarrow HCl + CH_2CHCH_2 \qquad \Delta_r H^{\ominus}_{298K} = -63.1 \text{ kJ mol}^{-1} \qquad (1)$$

produces HCl and a resonance-stabilized allyl (CH_2CHCH_2) radical. The abstraction of an allylic H-atom from the methyl group is exothermic, with $\Delta_r H^{\ominus}_{298K}$ = -63.1 kJ mol^{-1} calculated from tabulated heats of formation,[4-6] but removal of a vinylic H-atom is computed to be endothermic by more than 40 kJ mol^{-1},[7] and is not considered further. **Figure 1** shows a schematic potential energy surface (PES) for the reaction and indicates the possible reaction pathways. Direct hydrogen abstraction competes with delayed reaction following interaction of the Cl atom with the unsaturated C=C bond; 1-chloropropyl and 2-chloropropyl radicals resulting from addition of the Cl atom lie 80 kJ mol^{-1} lower in energy than the reactants. Reaction (1), and related reactions in larger alkenes, therefore present an opportunity to study the competition between direct and indirect reaction pathways.[6, 8-10] No transition state (TS) leads straight from the chloropropyl potential energy (PE) wells to HCl products,[7] but a TS has been suggested to connect these deep PE wells with the direct abstraction pathway.[6, 9]

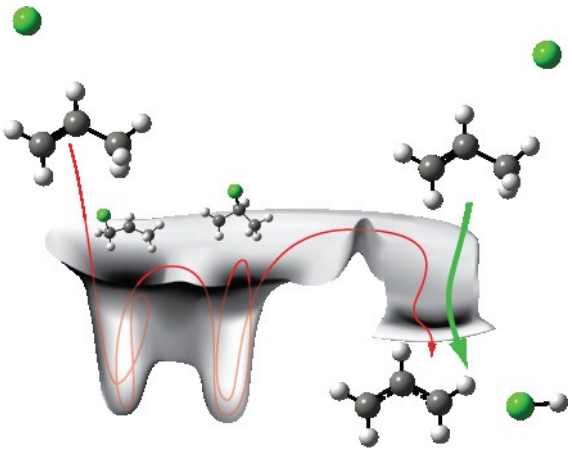

Figure 1: Schematic representation of the potential energy surface for reaction of a Cl atom (green) with a propene molecule. The green arrow shows the direct abstraction pathway forming HCl and an

allyl radical. The red arrow traces a reaction in which the Cl atom first adds to the C=C bond of propene, with interconversion between 1-chloropropyl and 2-chloropropyl radicals delaying escape to products.

Approximately half of the HCl molecules from reaction (1) form with one quantum of vibrational excitation, corresponding to 34.5 kJ mol^{-1} of internal energy.[8] On the basis of this and other evidence from their experimental measurements, Pilgrim and Taatjes proposed that the direct abstraction pathway dominates HCl production under thermal and low pressure (3-10 Torr) conditions. The indirect pathway was argued to favor statistical disposal of the excess energy among the degrees of freedom of the products. Transient infra-red spectroscopy of the HCl products of the related reaction of Cl atoms with 2,3-dimethylbut-2-ene in chloroform or tetrachloromethane solutions revealed 15-25% branching to HCl(v=1) products in the liquid phase.[11] Abou-Chahine *et al*. reasoned that the direct abstraction pathway is responsible for HCl production because rapid quenching of excess internal energy in a liquid environment would trap adduct chloroalkyl radicals in their associated potential energy wells.

The scattering of products from isolated collisions between Cl and propene, and the similar reactions of chlorine atoms with isobutene ($(CH_3)_2C=CH_2$) and 2,3-dimethylbut-2-ene ($(CH_3)_2C=C(CH_3)_2$), have been studied using velocity map imaging (VMI) of either the radical product[9] or its HCl partner.[6] Single-photon ionization and VMI of the isobutenyl radicals indicated a uniform scattering of products into all angles greater than 30°, when studied using crossed molecular beams of Cl atoms and isobutene at a collision energy of 28 kJ mol^{-1}.[9] Guided by electronic structure calculations of the energies of intermediates along the reaction path, Joalland *et al*. proposed large amplitude *roaming* dynamics connecting the 1- and 2-chloroalkyl PE wells with the H-atom abstraction pathway *via* a pathway lying lower in energy than the Cl + isobutene asymptote.[9] Preston *et al*. obtained complementary velocity map images of the HCl products of Cl + propene, isobutene and 2,3-dimethylbut-2-ene reactions, with

vibrational quantum-state resolution, that indicated a preference for forward scattering of HCl(v=1).[6] The mean collision energy in these experiments for the Cl + propene reaction was 27 kJ mol^{-1}. Interpretation of the scattering dynamics was guided by direct dynamics trajectory calculations using potential energies computed by density functional theory (DFT) methods at the B3LYP/6-31G(d,p) level. The computer simulations suggested only a minor contribution (less than 10%) from the indirect pathways in the Cl + propene reaction, with direct H-atom abstraction dominating the reaction. Both HCl(v=1) and (v=0) products were reported to derive from the direct abstraction pathway. However, calculations were limited to only 780 reactive trajectories because of the computational expense of the direct dynamics method.

We have computed and fitted a global PES for reaction (1) of Cl + propene to provide a more complete picture of the competition between direct and indirect dynamics in Cl + alkene reactions. Efficient computation of classical trajectories using this PES allows a comprehensive investigation of the reactive scattering and the branching between direct and addition-elimination pathways. We also examine the contribution of roaming dynamics to the overall reaction. The PES was generated using an empirical valence bond (EVB) fit [12-13] to high-level *ab initio* computed energies of reactants, products, and numerous intermediate species. This EVB-fitting methodology follows our recent reports of its use in quasi-classical trajectory (QCT) studies of the reactions of CN radicals with propane and cyclohexane,[14-15] F atoms with acetonitrile,[16-17] and Cl atoms with methane.[18] These former studies examined the dynamics of reactions that range from being close to thermoneutral to highly exothermic, but none featured a deep PE well corresponding to a reaction intermediate.

Section 2 of this paper describes the calculation of *ab initio* PE points and their fit to EVB functions. Section 3 presents the new PESs for the Cl + propene reaction and discusses the outcomes of quasi-classical trajectory calculations that simulate the quantum-state-specific scattering dynamics. We distinguish direct and indirect reaction mechanisms and explore their consequences for distribution of the excess energy among vibrational, rotational and translational motions of the products. The EVB

functionality allows us to switch off coupling terms connecting different regions of the PES, and we therefore contrast the dynamics on the global PES with dynamics constrained to the direct H-atom abstraction pathway. The outcomes are compared with available experimental measurements to test the quality of our computational description of the reaction dynamics.

2. Computational Details

2.1 Electronic Structure Calculations

There are several intermediates along the reaction profile that are necessary to include in our empirical valence bonding routine to describe accurately the reaction dynamics: separated reactants and products, 1-chloropropyl and 2-chloropropyl intermediates, and a Cl-propene π-adduct. These stationary points and transition-state geometries between them were optimized using restricted open-shell second-order Møller–Plesset perturbation theory (RMP2) employing Pople's 6-311G(d,p) basis set. Explicitly correlated coupled-cluster singles, doubles and perturbative triples (CCSD(T)-F12B) energies[19] were calculated for these geometries with the VDZ-F12 basis set.[20] Basis-set superposition error was assumed to be fully accounted for using explicitly correlated methods,[19] hence further corrections were not carried out. The 1-chloropropyl, 2-chloropropyl and π-adduct regions of the PES were further explored by calculating a grid of 300 points of CCSD(T)-F12B/VDZ-F12 energies at structures optimized at the RMP2/6-311G(d,p) level of theory, while keeping the C(1)–Cl and C(2)–Cl distances fixed. The MOLPRO suite of codes[21] was used to perform all of the electronic structure calculations. The effect of spin-orbit interactions, which should slightly stabilize the entrance channel, has been neglected here. The equilibrium geometries and structures are given in the Supporting Information.

Difficulties with converging the RMP2/6-311G(d,p) geometries along the direct abstraction pathway necessitated a different approach for this region of the PES. The direct H-abstraction channel was

instead mapped by computing CCSD(T)-F12B/VDZ-F12 energies at a set of structures generated by performing geometry optimization at the B3LYP/6-311G(d,p) level, fixing the reactive C–H and H–Cl distances and the C–H–Cl angle to 180°. At the RMP2/6-311G(d,p) level of theory, the value of this angle at the TS for direct abstraction is 176.2°; the applied constraint therefore does not unduly bias the results.

2.2 Empirical Valence Bond Description of the Reaction

Empirical valence bond theory fits to *ab initio* energy points provide the reactive PESs used in our trajectory calculations.[13] Implementation of the EVB method and construction of EVB PESs followed the procedures described in our recent study of the Cl + CH_4 reaction.[18] In the framework of EVB theory, the adiabatic reactive potential is obtained as the lowest eigenvalue of the EVB matrix, given on the left-hand side of Equation (1), whose entries are all functions of the coordinates of the system. For a given structure, the diagonal elements of the matrix, or *diabatic potentials*, correspond to the energy of that species with its bond connectivity. These diabatic potentials are expressed using molecular mechanics force fields. The off-diagonal elements describe the coupling between the various states and are usually simple functions of the relevant internal coordinates.[12-13, 22] A typical EVB eigenvalue equation assumes the form:

$$\begin{bmatrix} V_{R,R} & V_{R,P2} & V_{R,P3} & V_{R,P4} \\ V_{R,P2} & V_{P2,P2} + E_{P2} & 0 & 0 \\ V_{R,P3} & 0 & V_{P3,P3} + E_{P3} & 0 \\ V_{R,P4} & 0 & 0 & V_{P4,P4} + E_{P4} \end{bmatrix} \underline{c} = E\underline{c}, \qquad (1)$$

where $V_{R,R}$ is the force field function corresponding to the connectivity of the reactants *R*, $V_{Pj,Pi}$ and E_{Pj} are the force-field and reaction energy of the intermediate or product species P_j (here *j* = 2, 3 or 4 for Cl + propene), and $V_{R,Pi}$ is a coupling term between the reactants and the intermediate or product. Internal force-field parameters, such as those for stretch, bend, improper torsional, and torsional

motions were determined individually for each diabatic potential using the *ab initio* data in a manner described previously[18] and are listed in the Supporting Information.

The flexibility of the EVB method allows various parts of the global PES to be switched on or off by including or omitting the corresponding matrix elements in the EVB matrix. In the current study, three EVB model potentials were constructed. The *direct abstraction* EVB potential (EVB1) only included the reactant state, the three product states corresponding to HCl and the three equivalent radicals obtained by abstraction of one of the three methyl-group H atoms, and the couplings between them. The second EVB potential (EVB2) extends the EVB1 matrix by inclusion of the diabatic surfaces for the 1-chloropropyl and 2-chloropropyl radicals and couplings between the reactant state and these chloropropyl states, which are themselves coupled to one other. The most complete EVB potential, referred to here as the EVB3 or *full* PES, includes a further state corresponding to the π-adduct of the chlorine radical with the C=C double bond. This state is coupled to the reactant state, as well as to the 1-chloropropyl and 2-chloropropyl radical states. In the electronic structure calculations, the addition products only connect to bimolecular products *via* entrance-channel structures. We ensure this behaviour in the EVB surfaces by only coupling the three product states to the reactant state. **Figure 2** shows a diagram of these three EVB matrix arrangements. Both the EVB2 and EVB3 fits span the whole PES, but the omission (EVB2) or inclusion (EVB3) of the π-adduct state allows us to explore which of these two treatments models this region of configuration space better. Because of the omission of the π-adduct and associated couplings from the EVB2 PES, we refer to it as *restricted*.

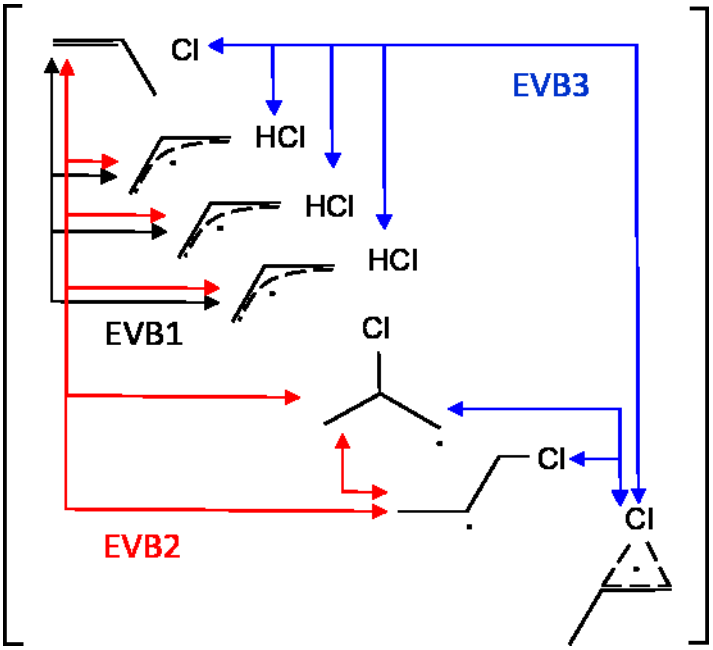

Figure 2: Pictorial representation of the three EVB matrices used in this work. Arrows indicate the couplings between the reactants, intermediates and products incorporated in the fits to for EVB1 (black), EVB2 (red) and EVB3 (blue) potential energy surfaces. See text for further details.

2.3 Parameterization of Terms in the EVB Matrix

The off-diagonal coupling terms in the EVB matrix are represented by one- or two-dimensional Gaussian functions. For the direct abstraction channel in EVB1, EVB2 and EVB3, these coupling terms depend on the methyl C–H and H–Cl distances. In EVB2, the reactant state and the chloropropyl radicals are coupled by 2D functions of the Cl–C(1) and Cl–C(2) distances. For EVB3, a 1D Gaussian function of the sum of the Cl–C(1) and Cl–C(2) distances describes the coupling between the reactants and the π-adduct. The Cl-atom is loosely bound to the double bond in the π-adduct, and this interaction is modelled by two Morse potentials between the chlorine and C(1) and C(2) atoms. In addition, Buckingham–Corner functions describe the non-bonded interactions between the Cl atom and the propene molecule. Furthermore, in EVB3 the π-adduct state is coupled to the 1-chloropropyl and 2-chloropropyl radical states with 1D Gaussian functions, taking the Cl–C(1) and Cl–C(2) distances

as their arguments. The Supporting Information provides further details about the potential energy functions and coupling parameters.

The CCSD(T)-F12B/VDZ-F12//B3LYP/6-311G(d,p) relaxed scan along the direct abstraction channel was fitted to give the EVB1 potential. The H–Cl, H–C and C–Cl van der Waals parameters, and the coupling parameters were allowed to vary during the fit. The H–H van der Waals parameters were taken from the CH_4+Cl potential we reported previously and were not altered.[18] In the fits to obtain the EVB2 and EVB3 potentials, all these parameters were kept fixed at the values obtained from the EVB1 fits, and the appropriate coupling terms for the Gaussian functions mentioned above were optimized. In the adopted procedure, we first fitted the CCSD(T)-F12B/VDZ-F12//RMP2/6-311G(d,p) *ab initio* points for structures with the Cl atom in proximity to the C=C double bond; these fits returned an initial estimate of the coupling terms connecting reagents to the chloropropyl radicals and the π-complex. Subsequently, trajectories propagated on this preliminary version of the EVB2 surface provided approximately 700 randomly selected geometries at which CCSD(T)-F12B/VDZ-F12 energies were computed. These additional points were incorporated into a refined fit to generate the final EVB2 and EVB3 expressions. There are 300 electronic structure points incorporated into the EVB1 potential energy surface, whereas EVB2 and EVB3 use 1000 points. All the fits used a methodology described previously.[18]

2.4 Quasi-Classical Trajectory Calculations

Separate sets of quasi-classical trajectory calculations were performed for each of the three EVB potentials. To propagate the trajectories, we used the VENUS suite of codes[23-24] that we previously interfaced with our EVB PES module.[18] The initial conditions of the trajectories were sampled as follows: the starting separation between the center of mass of the propene and the Cl atom was set to 6 Å; impact parameters were randomly sampled in the interval from 0 – 6 Å; the propene molecule was randomly oriented, and its zero-point vibrational energy was distributed among its internal degrees of freedom with orthant sampling as implemented in VENUS.[23] A trajectory time-step of 0.15

fs ensured conservation of energy to better than 99.9% at a collision energy of 28.1 kJ mol^{-1}, which corresponds to 0.2 kJ mol^{-1} absolute error of a total energy of 190 kJ mol^{-1} (chosen as the sum of the zero-point and collision energies). Histogram binning separated HCl products into final vibrational (*v*) and rotational (*j*) quantum states. Trajectories were discarded if the internal energies of either of the HCl and CH_2CHCH_2 products was below its respective zero-point energy.

3. Results and Discussion

The electronic structure calculations summarized in Section 2 provide a map of the potential energies for discrete structures of importance in the Cl + propene reaction, and a fit to an analytical function (chosen in our case to be the EVB description) generates a continuous potential energy surface. The quality of fits obtained using the EVB method and the topography of the energy landscape for the reaction are first examined before we turn to the chemical dynamics observed for our PESs using quasi-classical trajectory calculations.

3.1 Potential Energy Surfaces for the Cl + Propene Reaction

Figure 3 displays two-dimensional representations of selected regions of the PES for reaction (1), constructed from the *ab initio* electronic structure calculations and from EVB fits. We consider the three distinct EVB fits introduced above because they allow us to explore specific classes of reaction dynamics in the Cl + propene system.

The three fits incorporate different regions of the PES and thus require separate comparisons to the *ab initio* surface. Only the reactant and direct abstraction channels for the 3 equivalent methyl H atoms are included in the EVB1 potential. The energy of the separated reactants defines zero energy of the *ab initio* and all three EVB PESs. Along a relaxed scan of the hydrogen-abstraction path, the

EVB1 surface has an average unsigned error of 2.0 kJ mol^{-1} in the -60 to +80 kJ mol^{-1} region. The energy of the separated Cl + propene reactants was selected as the reference (zero energy) level for the *ab initio* and EVB surfaces, and the energy range over which we assess the fit accuracy extends from well above our chosen collision energy to a value corresponding to the product asymptote. The average fitting error compares favourably with our recent EVB fit of 300 *ab initio* points sampled from C_{3v} symmetry geometries for the $CH_4+Cl \rightarrow CH_3 + HCl$ reaction, which had a corresponding error of 1.2 kJ mol^{-1} in the 0 – 140 kJ mol^{-1} energy range.[18] The EVB2 and EVB3 surfaces deviate from the *ab initio* surface by an average of 12 kJ mol^{-1} and 10 kJ mol^{-1} respectively in the -90 to +120 kJ mol^{-1} potential energy region, which was chosen to encompass the radical PE wells incorporated in these PESs. Since the EVB2 and EVB3 matrices share the direct abstraction pathway submatrix with the EVB1 PES, the mean errors between the DA pathway *ab initio* scan and all three EVB surface fits to this region are almost identical.

The PESs in the region where the Cl atom is in proximity to the double bond can be partitioned into distinguishable sub-regions according to the position of the Cl atom. The 1-chloropropyl and 2-chloropropyl radicals appear as deep wells of depths -80 kJ mol^{-1} and -84 kJ mol^{-1} respectively. They are connected by a basin extending to 4 – 5 Å of separation between the Cl atom and the C=C bond. This basin, evident in panels e, g and f of **Fig. 3**, corresponds to the π-complex. When the EVB matrix elements describing the covalent Cl-double bond interactions are omitted from the potential in the EVB1 model, the Cl atom only experiences van der Waals interactions with the $H_2C=CH-$ moiety, as shown by the missing wells in **Fig. 3(f)**. The EVB2 potential reproduces the two chloropropyl wells (**Fig 3(g)**); however, the region between them has two extra barriers compared to the *ab initio* potential (**Fig. 3(e)**). The breadth of the π-complex region is also smaller in the EVB2 fit compared to the *ab initio* grid of points. The inclusion of the π-complex and its associated coupling terms in the EVB3 matrix removes the barriers and widens the π-complex basin region, in evidence in **Fig. 3(h)**.

Table 1 compares the energies of various stationary points on the *ab initio* and EVB1, EVB2 and EVB3 PESs. The *ab initio* and three EVB PES abstraction reaction energies are identical. The energies of the direct abstraction TSs on the three EVB surfaces are close to that of the *ab initio* PES, but are all lower by 5 kJ mol^{-1}. The 1-chloropropyl and 2-chloropropyl wells in EVB2 and EVB3 are slightly deeper than the corresponding *ab initio* energies.

Table 1: The *ab initio* CCSD(T)-F12B/VDZ-F12//RMP2/6-311G(d,p) and EVB reaction and transition-state energies.

	Energy / (kJ mol^{-1})			
Reaction / Species	*ab initio*	EVB1	EVB2	EVB3
Reactants to allyl + HCl	-52.4	-52.4	-52.4	-52.4
Reactants to 1-chloropropyl	-89.1		-91.6	-92.4
Reactants to 2-chloropropyl	-84.8		-92.8	-102.9
Reactants to π-complex	-46.1			-46.1
Direct abstraction TS	27.2	22.6	22.6	22.6

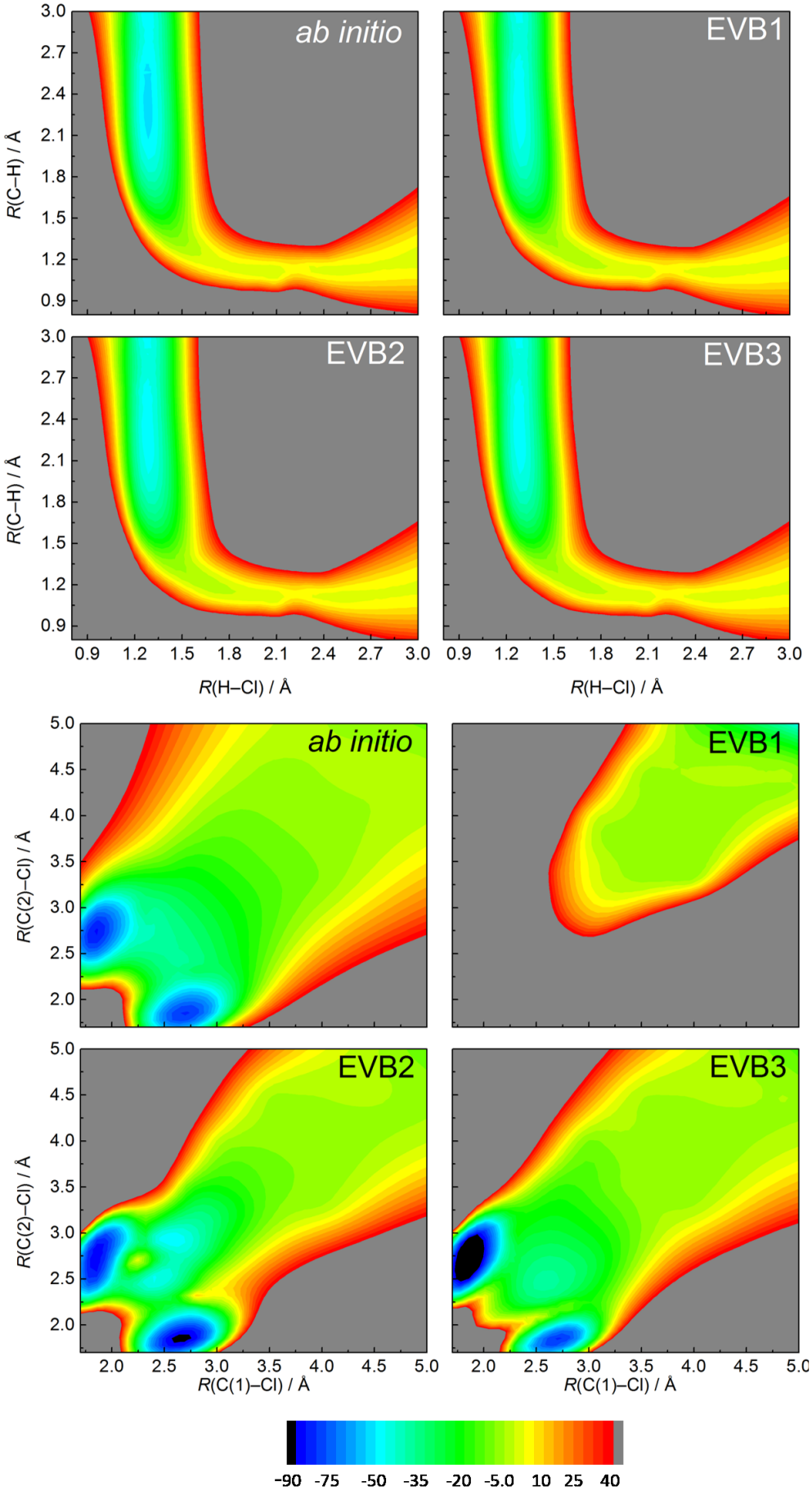
ab initio
EVB1
EVB2
EVB3
R(C–H) / Å
R(H–Cl) / Å
R(C(2)–Cl) / Å
R(C(1)–Cl) / Å
-90 -75 -50 -35 -20 -5.0 10 25 40

Figure 3: Two-dimensional cuts through the potential energy surface for the Cl + propene reaction. Panels (a) – (d): collinear relaxed scans along the C–H–Cl coordinate. The reactants are located in the bottom right corner of each panel. The *ab initio* CCSD(T)-F12B/VDZ-F12//B3LYP/6-311G(d,p) scans are shown in panel (a) and are compared with the EVB1 (b), EVB2 (c), and full EVB3 (d) fitted surfaces. Panels (e) - (h): relaxed scans around the region of interaction of the Cl atom with the C=C double bond. The distances between the first and the second carbon atoms and the Cl atom were kept fixed. The 1-chloropropyl radical is on the extreme left of each panel, and the 2-chloropropyl radical is located at the bottom of each panel. The *ab initio* CCSD(T)-F12B/VDZ-F12//RMP2/6-311G(d,p) scans are shown in panel (e), and are again compared to the EVB1 (f), EVB2 (g) and EVB3 (h) fits.

3.2 Quasi-Classical Trajectory Calculations

Quasi-classical trajectory calculations were propagated for the Cl + propene reaction using the VENUS package[23-24] and the methodology summarized in Section 2. These QCT calculations were performed using the EVB1, EVB2 and EVB3 PESs to contrast the dynamics on a global PES with those on PESs with restrictions imposed on the allowed reaction pathways. Sufficient numbers of reactive trajectories were propagated to extract distributions of the internal energies of the reaction products, distributions of product scattering angles, and to analyze the propensities for direct and indirect reaction mechanisms. These results are presented here, with comparison to experimental measurements where available. Of the 1.0 million (on the EVB1 PES), 1.6 million (EVB2 PES) and 1.6 million (EVB3 PES) trajectories propagated, 64,000, 105,000, and 27,000 respectively led to HCl + allyl radical products. Of these reactive trajectories, 34,000, 56,000, and 14,000 satisfied the criterion of vibrational energies greater than the zero-point vibrational energies of both products and were deemed successful. Only these last subsets of trajectories were further analyzed. The similar numbers of reactive trajectories suggest that the reaction cross sections are comparable for all of the three EVB surfaces, regardless of whether the interaction between the Cl atom and the C=C double bond is included and how it is treated. In many trajectories on the EVB2 and EVB3 surfaces, the Cl atom is attracted to the π-orbitals of the C=C bond, samples the 1-chloro and 2-chloropropyl potential wells, but escapes without undergoing chemical reaction.

3.2.1 Product HCl Rotational Energy Distributions

Reactions of Cl atoms with alkanes typically produce HCl that is rotationally cold because of the preferred collinear Cl-H-C geometry in the transition state[25] and the weakness of anisotropic post-TS interactions between the separating HCl and alkyl radical products.[26] However, a recent experimental report of the dynamics of the Cl + propene reaction indicated that the HCl products were formed with considerable rotational excitation.[6] This observation is borne out by our trajectory calculations. The plots in **Figure 4** of relative populations of HCl in different rotational levels show distributions of rotational angular momentum quantum numbers, j, peaking between 8 and 12, with few products formed with $j < 5$. Computed distributions are presented for all HCl products, and for those formed in vibrational levels $v = 0$ and $v = 1$. These distributions show little variation with the choice of EVB1, EVB2 and EVB3 PES suggesting features common to all three PESs control the rotational energy and angular momentum of the HCl product. We separate direct and indirect reactions by their time to completion t_{react} (defined by product separation reaching 5 Å). Sampling the 1- and 2-chloropropyl regions of the PES takes more time, and we show in Section 3.2.4 that separation into regimes $t_{react} <$ 1 ps and $t_{react} > 1$ ps isolates these two reaction mechanisms for further analysis. The distribution of HCl rotational populations for the indirect trajectories is shifted slightly to higher j than the average over all trajectories. As discussed below, trajectories with $t_{react} > 1$ ps represent only a small fraction of all successful reactions.

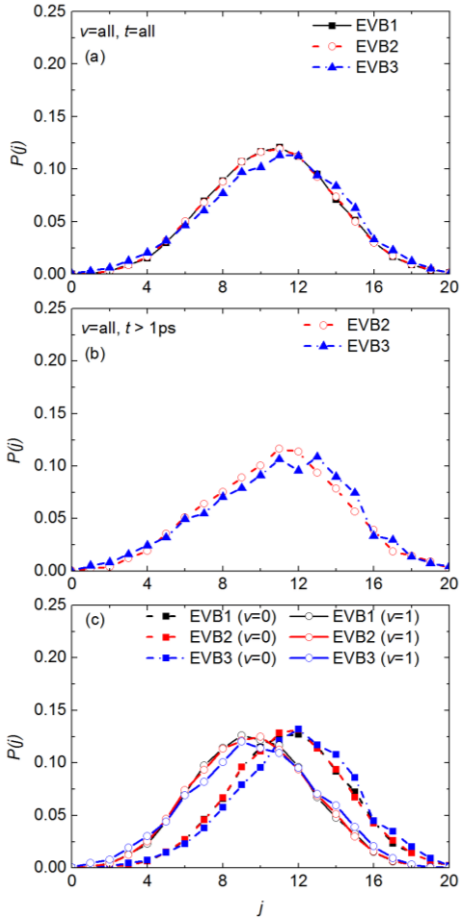

Figure 4: Rotational level population distributions of HCl from the Cl + propene reaction computed using the direct abstraction EVB1 (black), restricted EVB2 (red) and full EVB3 (blue) potential energy surfaces. (a) Rotational distribution for all HCl product vibrational quantum states from reactive trajectories of all durations. (b) As for panel (a), but including only the outcomes of trajectories lasting more than 1 ps. (c) HCl(v=0) and (v=1) product rotational distributions.

Fig. 4(c) illustrates how the maximum in the HCl rotational distribution shifts to lower j when the HCl forms in v=1. For both HCl(v=0) and (v=1) products, the maximum in this distribution corresponds to approximately 20% of the available energy entering rotational motion of the HCl, suggesting no significant changes to the reaction dynamics leading to these two HCl(v) channels. The Boltzmann plots displayed in **Figure 5** show that these rotational distributions are not well described by a single temperature. The plots are presented for trajectories computed on the EVB3 PES, with almost

identical results obtained for the EVB1 and EVB2 surfaces as shown in the Supporting Information. At least two regimes are evident in **Fig. 5**, with an inverted distribution at low *j* and a higher-*j* region approximated by a temperature of 700 – 900 K. Preston *et al*. reported that the HCl(*v*=0) products of the Cl + propene reaction populate rotational levels with a distribution described by a rotational temperature of 630 K and a much hotter component ill-described by a single temperature, whereas HCl(*v*=1) products are significantly rotationally colder, with T_{rot} = 200 K.[6] Our calculations are therefore in partial agreement with the experimental measurements for HCl(*v*=0) but appear to over-estimate the degree of rotational excitation of HCl(*v*=1) products. The small fraction of trajectories lasting longer than 1 ps favour a higher rotational temperature of the HCl (compare the blue triangles and black squares in **Fig. 5**, or the green triangles and red circles), which may account for the experimental observation of a second, rotationally more excited component. The decomposition of experimental data into direct and indirect pathways based on the degree of HCl rotational excitation is not, however, as clear-cut as our prior direct dynamics simulations suggested.[6]

The extent of HCl rotational excitation differs markedly from Cl + alkane reaction outcomes,[25] despite both mechanisms involving H-atom abstraction from an sp^3 hybridized C-atom. The greater release of energy in the Cl + propene reaction must be in part responsible for this difference, although angular anisotropy in the post-transition-state region may also contribute.[26]

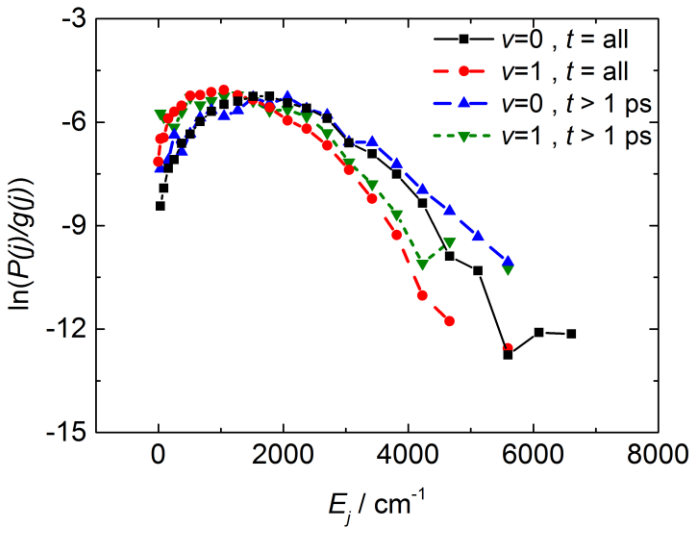

Figure 5: Boltzmann plots of the rotational energy distributions obtained from trajectories propagated on the EVB3. An analysis of all reactive trajectories gives the rotational distributions shown for HCl(v=0) (■)and HCl (v=1) (●) The corresponding distributions for the small subset of trajectories taking longer than 1 ps to complete are also shown for HCl(v=0) (▲) and HCl(v=1) (▼).

3.2.2 Product HCl Vibrational Energy Distributions

Pilgrim and Taatjes reported an experimental determination for reaction (1) of Cl with propene under thermalized conditions at 293 K of the branching to HCl(v=1) and HCl(v=0) of 0.46 (v=1) : 0.54 (v=0) with an uncertainty of ±0.06.[8] This ratio is reproduced remarkably well by our simulations, which compute a ratio of 0.02 (v =2) : 0.43 (v=1) : 0.55 (v=0) as shown in **Figure 5**. Again, these ratios are insensitive to the choice of EVB PES, and they change only modestly when reactions longer than 1 ps in duration are considered in isolation. The vibrational excitation of approximately half the HCl products reflects the early transition state to the direct abstraction pathway, which is a consequence of the large exothermicity of the reaction. The mean collision energy in the 293-K experiments is 2.4 kJ mol^{-1} whereas our calculations were performed at a collision energy of 27 kJ mol^{-1}, but the agreement between vibrational branching ratios suggests that the position of the transition state is

more important in determining the product vibrational excitation than is the collision energy (at least, for conditions in which the collision energy remains less than the exothermicity of the reaction).

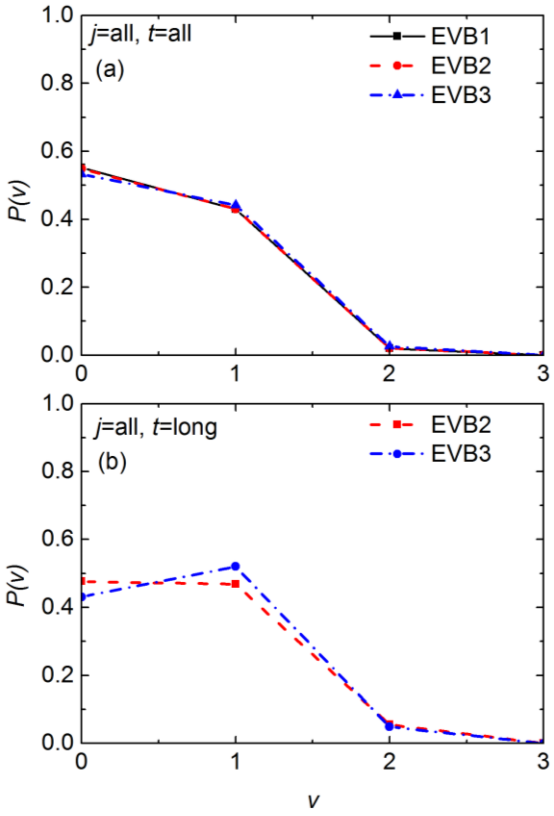

Figure 6: Vibrational level population distributions for the HCl products of reaction of Cl with propene. The distributions were obtained from trajectories propagated on the direct abstraction EVB1 (black), restricted EVB2 (red) and full EVB3 (blue) potential energy surfaces, and are averaged over all rotational levels of HCl. Panel (a) shows the outcomes obtained by analysis of trajectories of all durations, and panel (b) shows the vibrational distribution from the small fraction of trajectories lasting more than 1 ps.

3.2.3 Product Angular Scattering

Experimental studies of the reaction of Cl atoms with propene, and the related Cl + isobutene and Cl + 2,3-dimethylbut-2-ene reactions, have also measured the angular scattering of the reaction products. Crossed molecular beam and velocity map imaging studies by Suits and co-workers probed

the scattering of the isobutenyl radical product of reaction of Cl atoms with isobutene.[9-10] Their method of detection did not provide any product ro-vibrational quantum-state resolution, but Preston *et al*. reported dual-beam and VMI studies of the Cl + propene, Cl + isobutene and Cl + 2,3-dimethylbut-2-ene reactions with imaging of the velocities of HCl(v=1, j=2-4) products.[6] The crossed molecular beam study of Suits and workers observed nearly uniform product scattering over angles from 30-180^o (but could not resolve forward scattering into angles below 30^o) whereas Preston *et al*. reported a preference for forward scattering of the products in the centre-of-mass frame, albeit with broad angular scattering extending back to 120^o.

The computed scattering distributions plotted in **Figure 7** for the full EVB PES are qualitatively in good agreement with the experimental results of Preston *et al.*, as well as their direct dynamics simulations, showing a preference for forward scattering of HCl(v=1) products (averaged over all j) and only weak flux into the backward hemisphere. The same behavior persists when all product HCl vibrational levels are included in the averaging. The dual-beam scattering experiments are vulnerable to undercounting the most strongly backward scattered products;[27-28] when this experimental limitation is taken into account, the agreement with the calculations is very satisfactory. The subset of trajectories with $t_{react} > 1$ ps exhibit almost equal propensities for forward and backward scattering, which is expected when the lifetime of any reaction intermediate exceeds its rotational period.[29]

Trajectory calculations using the direct abstraction EVB1 and the restricted EVB2 PESs show a weaker preference for forward scattering than for the EVB3 PES, indicating that the additional couplings included in the EVB matrix for the EVB3 PES are important for determining the scattering distribution and thus are necessary to describe correctly the reactive surface. Examination of the distribution of impact parameters leading to reactive events affords further insights: the peak in the impact parameter distribution is shifted by about 1 Å to larger values for the EVB3 potential relative to the direct abstraction EVB1 and restricted EVB2 potentials. This shift arises because the attractive potential extends further from the carbon framework when the π-complex is included in the EVB

matrix (e.g. see **Fig. 3(h)**). As a consequence, a greater number of trajectories with larger impact parameters lead to reactive collisions *via* the direct stripping mechanism we highlight below. The perhaps non-intuitive increase of direct abstraction reactions results from a more complete description of the intermediate pathways, thereby causing more pronounced forward scattering.

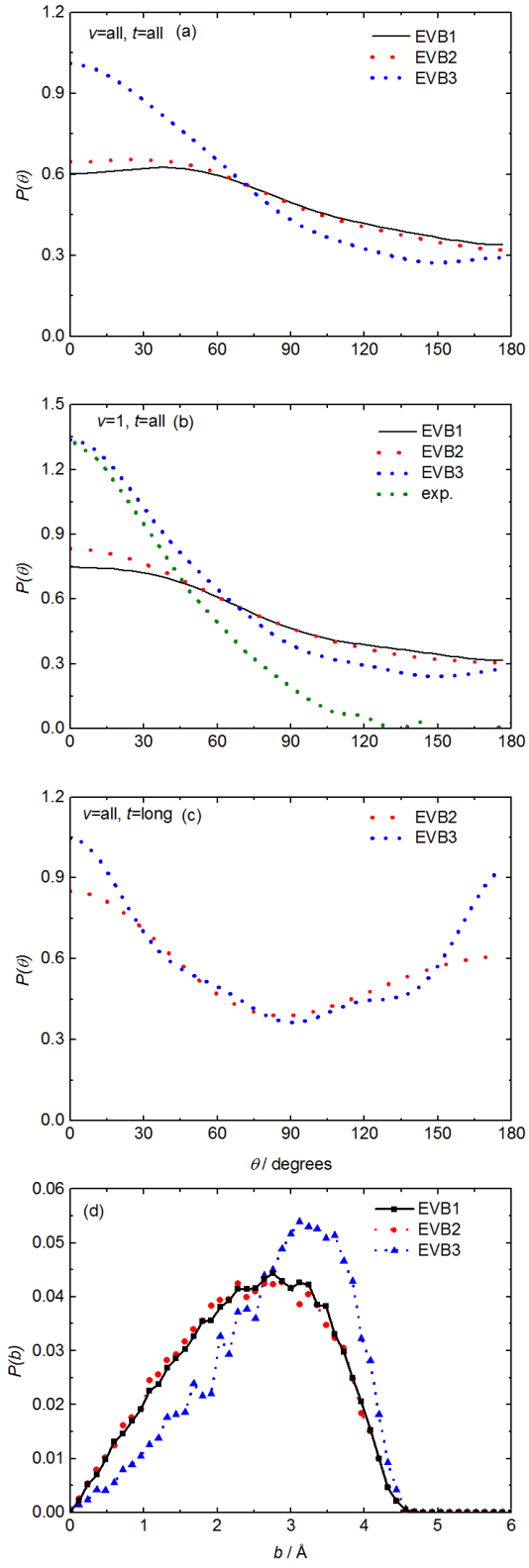

Figure 7: Angular scattering distributions of HCl products of the Cl + propene reaction in the center-of-mass reference frame, computed using the direct abstraction EVB1 (black), restricted EVB2 (red) and full EVB3 (blue) potential energy surfaces: (a) averaged over all reactive trajectories and all product HCl rotational and

vibrational quantum states ; (b) for HCl(v=1) only, averaged over rotational levels; (c) for trajectories lasting more than 1 ps, with averaging over HCl vibrational and rotational levels. Panel (d) shows the probability distribution function of the impact parameters for reactive trajectories on the three EVB PESs with the same color coding.

3.2.4 Direct and Indirect Pathways

Reactions of Cl atoms with alkanes are dominated by direct H-atom abstraction pathways,[25] but the introduction of a C=C bond functionality opens up new mechanistic possibilities. Foremost among these are addition to the C=C bond to form a chloroalkyl radical, followed by elimination of Cl or HCl, and *roaming* dynamics corresponding to large-amplitude motions of the Cl atom about the alkene. Both Joalland *et al*.[9] and we[6] previously identified a pathway connecting the chloroalkyl and direct abstraction regions of the PES for reactions of Cl with alkenes. The influence of passage between these regions on the overall reaction dynamics, however, remained uncertain. Crossed molecular beam scattering results hinted at an important role for delayed dynamics associated with interaction of the Cl atom with the C=C bond,[9-10, 30] whereas our experimental studies of reactive scattering suggested the direct abstraction pathway was the more significant.[6] This latter deduction was supported by the outcomes of a small number of direct dynamics trajectories, computed on-the-fly using B3LYP/6-31G(d,p) potential energies.[6] The much larger number of trajectories that can be computed using our EVB PESs now allows us to address this question with greater confidence.

The proportion of simulations surviving longer than 1 ps is about 16% for EVB2 and about 10% for EVB3. These *long-lived* trajectories form energized 1-chloropropyl of 2-chloropropyl radicals or π-adducts. The majority then dissociate back to reactants, but some do dissociate to HCl + allyl radical *via* an indirect mechanism. Non-reactive trajectories that instead complete in less than 1 ps are labelled as *by-passing*. The fractions of long-lived reactive and non-reactive trajectories are shown in **Table 2** alongside those for other mechanisms. The small number of reactive compared to non-

reactive trajectories is in part a consequence of imposing product zero-point-energy criteria to identify successful trajectories. In the Table, the divisions into reactive and non-reactive outcomes are further sub-divided according to their durations.

Table 2: Fractions of Cl + Propene Trajectories Separated by Reaction Mechanism.

Trajectory type		PES EVB2	PES EVB3
Reactive	All	0.066	0.017
	Direct	0.937	0.909
	Indirect	0.063	0.091
Non-reactive	All	0.934	0.983
	By-passing	0.840	0.900
	Long-lived	0.160	0.100

Figure 8 shows further imprints of the reaction time t_{react} on dynamical aspects of the Cl + propene reaction. The figure displays an analysis of the number of reactive trajectories of different durations (**Fig. 8 (a)** and **(b)**), and variations in average scattering angles (**Fig. 8 (c)** and **(d)**) and impact parameters (**Fig. 8 (e)** and **(f)**) with trajectory duration. A substantial majority of the trajectories completes within 500 fs, and these short-lived trajectories are associated with direct H-atom abstraction pathways avoiding delaying interactions with the C=C region in propene. Fewer than 10% of reactive trajectories exceed t_{react} = 1 ps, and of these, some are delayed by up to 250 ps (**Fig. 8(a)**). Among a random selection of long-lived trajectories we have inspected, many involve formation of 1-chloropropyl or 2-chloropropyl radicals. The predominance of direct abstraction agrees with the deduction by Pilgrim and Taatjes from their spectroscopic study of the reaction outcomes.[8] The shortest duration trajectories have small impact parameters (**Fig. 8(f)**) and correspond to direct rebound dynamics with HCl scattering into the backward hemisphere (θ>90^o) (**Fig. 8(d)**). Larger impact parameters provide a regime of slightly longer duration trajectories simply because of the greater distances traversed in the passage from reagents to forward scattered products. For time durations up to 500 fs, the scattering therefore favours the forward hemisphere (θ<90^o). Thereafter, the

average scattering angle tends towards 90° as long-lived complexes contribute to the reaction (**Fig. 8(c)** and **(d)**). A range of impact parameters can lead to the formation of these complexes, consequently a mean value of the impact parameter of between 1 and 2 Å is obtained for time delays greater than 1 ps (**Fig. 8(e)**).

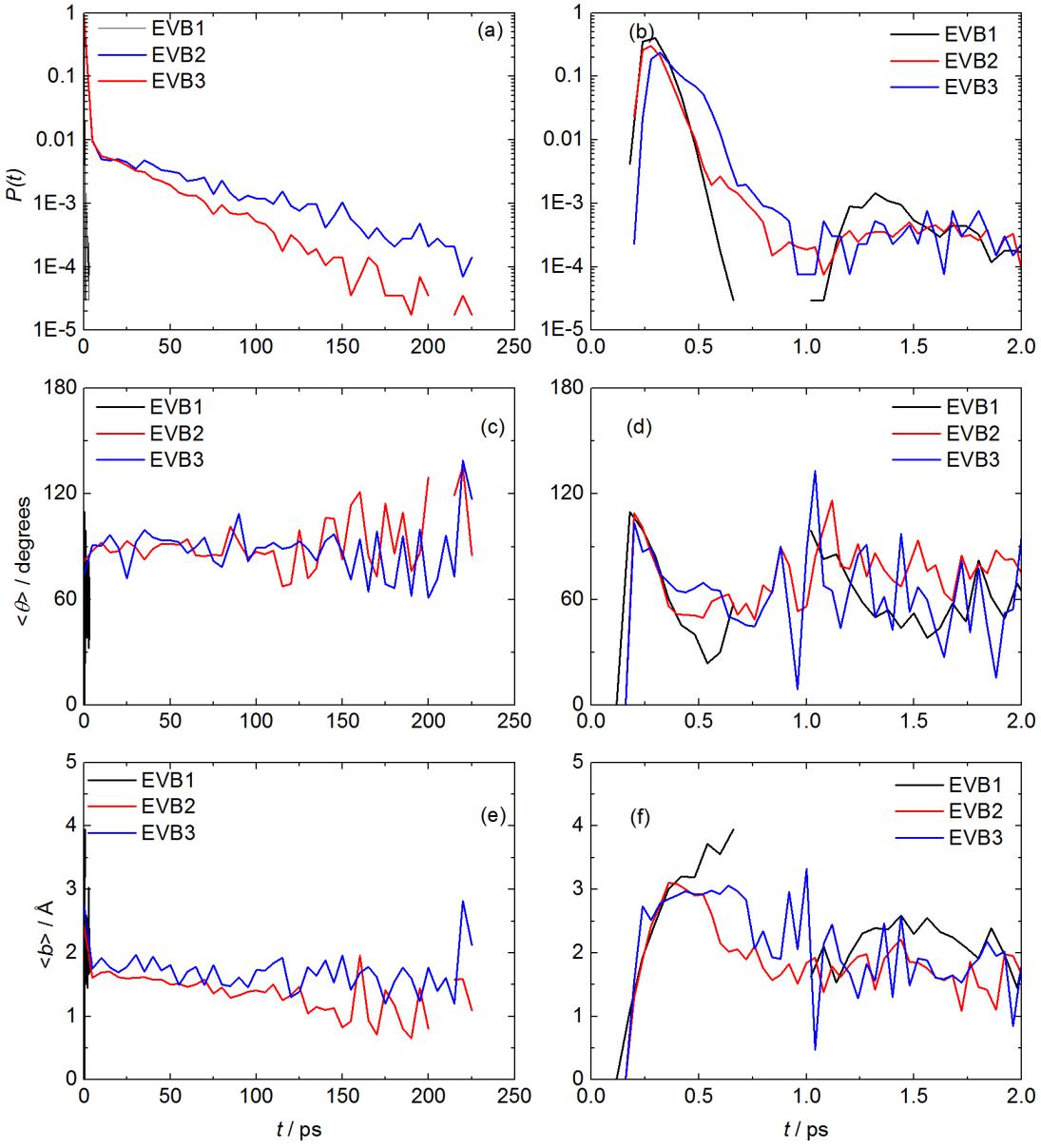

Figure 8: Dependence of selected properties of the reaction on duration of the trajectories for times up to 250 ps (left hand column), and with an expanded view of the first 2 ps (right hand column). Panels (a) and (b): reaction probability. Panels (c) and (d): average scattering angle. Panels (e) and

(f): average impact parameter. Results are shown for the three PESs: EVB1 (black); EVB2 (red); EVB3 (blue).

The small fraction of trajectories sampling the PE wells of the chloropropyl radicals and the short (<250 ps) lifetimes of these complexes suggest that the outcomes of the Cl + propene reaction will be insensitive to applied bath-gas pressure. Only at pressures of a few bar or above will quenching collisions with the bath gas compete successfully with the dissociation of the internally excited chloropropyl radicals.

3.2.5 Visualization of Trajectory Types

Animated examples of trajectories of different time durations are available as Supporting Information, and **Figure 9** presents schematic illustrations of the different mechanisms we observe. The predominant pathway is direct abstraction of an H-atom from the methyl group, shown in panels (a) and (b), which is analogous to the mechanisms of reaction of Cl atoms with alkanes.[25] Interaction with the C=C double bond, shown in panels (c) and (d), is a minor contributor despite being energetically favorable. Those chlorine atoms that do wander into close proximity with the C=C bond experience alternative reaction mechanisms including addition prior to H-atom abstraction, and large amplitude motions of either Cl or HCl around the carbon framework.

The pathway connecting the 1-chloropropyl and 2-chloropropyl radical adducts to reaction products requires almost, but not necessarily complete separation to the energy of the Cl + propene asymptote, as shown in **Figure 1**. This connection to the direct abstraction region of the PES leads Cl atoms away from interactions with the C=C bond. The signatures in the HCl product of the dynamics of Cl atoms that follow this more circuitous route are therefore difficult to distinguish from those of the direct H-atom abstraction pathway. Both HCl (v=0 and 1) products form via both mechanisms, and the population distributions over HCl rotational levels are very similar. Preston *et al*.[6] proposed that the

degree of rotational excitation of HCl could be used to discriminate between the two reaction mechanisms, but the current calculations suggest otherwise. Moreover, our trajectory calculations indicate that the roaming pathway proposed by Joalland *et al*. in reactions of Cl atoms with isobutene,[9] a reaction expected to be mechanistically very similar to that of Cl atoms with propene, is only a minor contributor to the pathways for reaction (1).

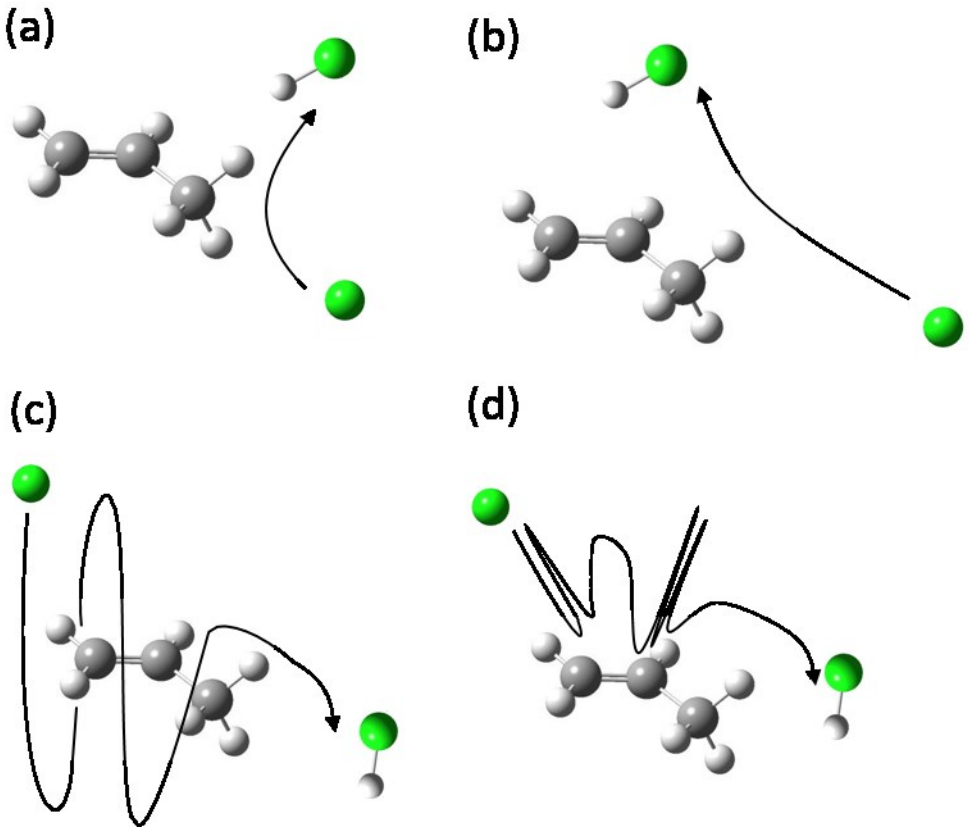

Figure 9: Sketches of characteristic reaction mechanisms observed from trajectories. (a) rebound direct abstraction leading to predominantly backward scattered products, and usually associated with small impact parameter collisions. (b) Stripping direct abstraction in which the Cl atom abstracts an H atom when passing by the propene molecule at larger impact parameters, giving smaller scattering angles. (c) Roaming abstraction, with the Cl atom orbiting around the propene molecule before detaching an H atom. (d) Delayed abstraction, in which the Cl atom adds to one or other of the carbon atoms making up the double bond and alternates between the two before abstracting an H atom if its momentum carries it towards the methyl group when the addition complex falls apart.

The competing mechanisms of reaction illustrated in **Figure 9** are now explored in further detail. Defining a set of internal coordinates helps monitor the movement of the Cl atom with respect to three carbon atoms. The coordinates illustrated in **Figure 10** are the distance *r* between the Cl atom and the centre of the C(1) − C(2) bond; the distance atom $r_{Cl\text{-}C(2)}$ between the Cl atom and central carbon; the Jacobi angle γ between *r* and the C=C bond (with γ = 0 towards the central C atom); and the dihedral angle χ between *r* and the plane of the three carbon atoms of propene. **Figure 10** also illustrates the different interactions experienced by the Cl and propene during extended trajectories. The trajectory plotted in **Fig. 10(b)** can be sub-divided into two regimes: formation of internally excited 1-chloropropyl and 2-chloropropyl radicals and exchange between them, and roaming of the Cl atom about the propene molecule. Preference for γ>90^o and 2.5 Å $\leq r_{Cl\text{-}C(2)} \leq$ 3.0 Å indicate that the system favors the 1-chloropropyl radical state. Jumps to smaller values of $r_{Cl\text{-}C(2)}$ and γ<90^o indicate transitions to 2-chloropropyl. When sufficient energy is transferred to coordinates involving displacement of the Cl atom, the atom starts to roam around the propene moiety, indicated by the large amplitude variations of the three internal coordinates at late times after the broken abscissa. Finally, an abstraction reaction takes place to form HCl and allyl radicals. A purely roaming abstraction trajectory is shown in panels (c) and (d) of **Figure 10**.

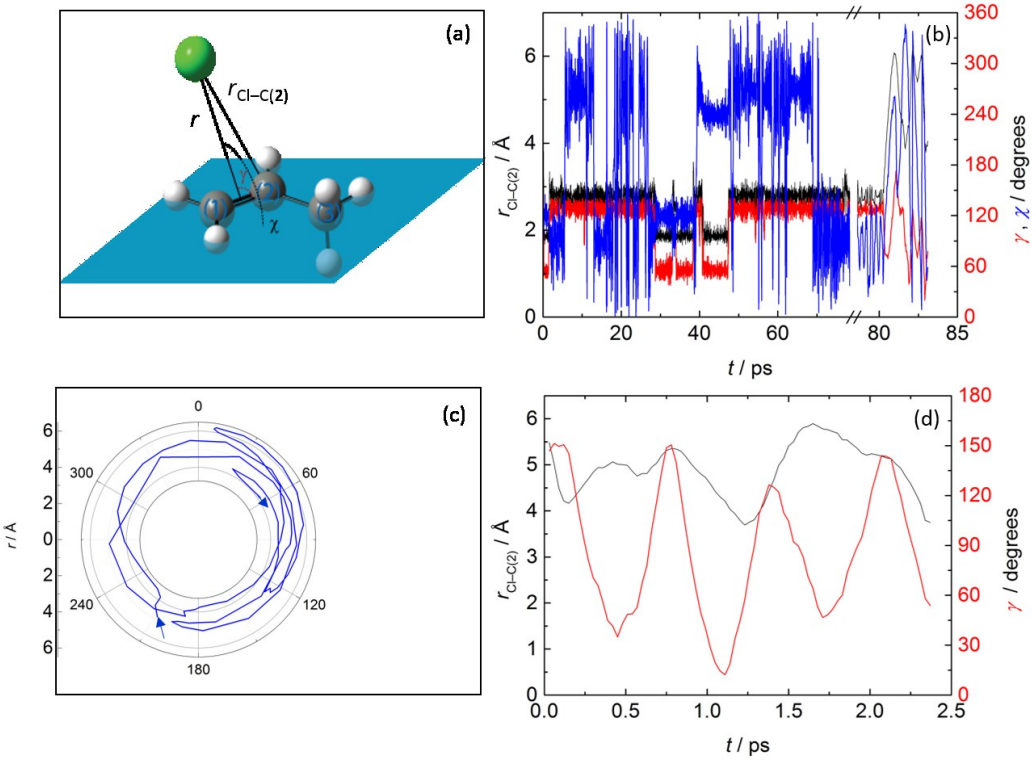

Figure 10: Examples of the dynamics contributing to long-lived but rare types of trajectory. (a) The internal coordinate system defined to describe the motion of the Cl atom relative to the three carbon atoms of propene. (b) A trajectory in which the HCl is formed by delayed abstraction via 1-chloropropyl and 2-chloropropyl complexes; the plot shows the changes in $r_{Cl-C(2)}$ (black) and in the angles γ (red) and χ (blue). For the first 70 ps, the Cl atom hops between the two potential energy wells of 1- and 2-chloropropyl. The split abscissa highlights the extended $r_{Cl-C(2)}$ distances as Cl roams around the molecule for about 3 ps before the H atom is abstracted. Panels (c) and (d) show two different representations of roaming dynamics in a different trajectory; (c) time variation of the dihedral angle χ illustrating how the Cl atom orbits the carbon backbone of the propene before removing an H atom from the methyl group; (d) concomitant changes to $r_{Cl-C(2)}$ (black) and γ (red).

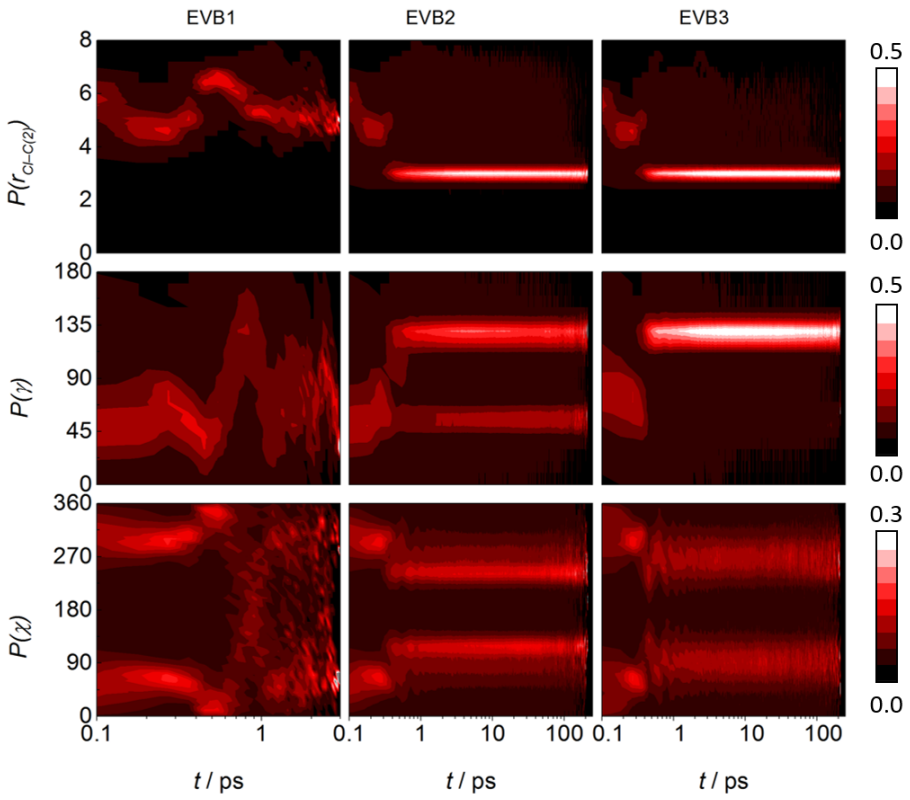

Figure 11: Probability distributions of the internal coordinates $r_{Cl\text{-}C(2)}$, γ and χ with the time as the reaction progresses for encounters between Cl atoms and propene molecules. The three columns are for the direct abstraction (EVB1, left), restricted EVB (EVB2, center) and full EVB (EVB3, right) potential energy surfaces. The coordinates plotted are $r_{Cl\text{-}C(2)}$ (top row), γ (middle row) and χ (bottom row), as defined in **Fig. 10(a)** and the main text. Each vertical slice in a panel corresponds to a time bin and is normalized to unity.

Further representations of the outcomes of the trajectory calculations provide additional mechanistic insights. For example, **Figure 11** shows plots of the variation with time as the reaction progresses of the mean values of the three coordinates: $r_{Cl–C(2)}$, γ, and χ (see **Fig. 10(a)**) for trajectories computed on each of the three EVB surfaces. The large Cl–C(2) separation during the first few hundred femtoseconds is characteristic of rebound reactive collisions in which the Cl atom does not come close to the middle carbon atom. The mean value of $r_{Cl–C(2)}$ gradually shifts toward smaller values of about 4 Å which is indicative of stripping dynamics during which the reactant Cl atom and the product HCl pass by the carbon frame of the molecule over times in the range 300–500 fs. Restriction of the dihedral angle χ to the ranges 0–90° and 270–360° is purely geometrical in origin, because of the orientation

of the methyl group with respect to the C(1)=C(2) bond. The 1-chloropropyl and 2-chloropropyl radicals show up as horizontal bands in the angle γ after 700 fs for calculations using the EVB2 and EVB3 PESs which include interaction with the double-bond region. The $\bar{\gamma}$ band centred around 135° corresponds to the 1-chloro isomer (the anti-Markovnikov addition), whereas the much weaker band around 45° indicates the 2-chloro (Markovnikov) isomer. The 2-chloro isomer is even less favored in trajectories computed using the full EVB surface (EVB3).

The mobility of the Cl-atom between isomers and around the carbon-atom framework makes the distributions of the dihedral angle $\bar{\chi}$ somewhat diffuse. Despite more than 100 kJ mol^{-1} of excess energy in these radicals, however, the χ values are mostly distributed around the the RMP2/6-311G(d,p) equilibrium dihedral angles of 80°/280° and 120°/240° for the 1-chloropropyl and 2-chloropropyl radicals respectively. For reactions lasting longer than 700 fs, the average fractions of time spent as 1-chloro or 2-chloro radicals, or undergoing roaming are 93%, 4% and 3% respectively for the restricted EVB2 potential. The corresponding ratios are 97%, 1.6% and 1.4% on the full EVB3 surface.

The low probability of reaction *via* mechanisms other than direct H-atom abstraction provides some rationale for the observation of HCl(v=0 and 1) products of the Cl + 2,3-dimethylbut-2-ene reaction in solution in chloroform or carbon tetrachloride.[11] This reaction is mechanistically similar to the Cl + propene reaction studied here. Collisions with solvent molecules can stabilize the chloroalkyl radicals formed by addition of the Cl atom to the central C=C bond of the alkene, but our quasi-classical trajectory calculations indicate that only a small fraction of trajectories sample this addition pathway. For the Cl + 2,3-dimethylbut-2-ene reaction, in which four times as many methyl H atoms surround the C=C bond, direct abstraction will prevail even more. The available evidence points towards dynamics of the reactions in these chlorinated solvents that are little changed from those for isolated collisions in the gas phase; direct H-atom abstraction dominates, with significant branching to

vibrationally hot HCl. The similarities and differences are currently under further examination in simulations that use the EVB3 PES and incorporate explicit solvent molecules.

4. Conclusions

A global potential energy surface has been created to describe the reaction of Cl atoms with propene. The PES is based on approximately 1000 high level *ab initio* potential energies points corresponding to different geometries of the nuclei. These points are fitted using an empirical valence bond model that provides a continuous potential energy function for quasi-classical trajectory calculations. The full PES includes a direct H-atom abstraction pathway, two deep minima associated with the 1-chloropropyl and 2-chloropropyl radicals, and a pathway linking these regions. Reduced versions of the EVB model fit allow exploration of the significance of different regions of the PES on the reaction dynamics, a strength of the EVB approach.

Analysis of 56,000, 27,000, 14,000 zero-point energy conserving reactive trajectories, run on three differently constructed EVB surfaces, reveals several interesting facets of the dynamics of this Cl + alkene reaction. The predominant dynamics are similar to those of Cl atoms with alkanes, even though propene contains only a single sp^3 hybridized carbon atom. Interaction of the Cl atom with the C=C double bond contributes more complex dynamical pathways. In these longer-lived reactions, the Cl atom adds temporarily to one or other of the unsaturated carbon atoms, and can roam around the propene framework before removing an allylic hydrogen atom. Although the sp^2 hybridized carbon atoms and their vinylic H atoms constitute about half of the geometric area of the propene molecule, fewer than 10% of reactive encounters follow these indirect reaction routes. The majority of the reactive events lead to forward scattering of HCl products, which form in either v=0 or 1 with approximately equal propensity. These HCl molecules are rotationally hotter than in Cl + alkane reactions. These computational outcomes are in qualitative, and in some cases quantitative

agreement with experimental measurements of this reaction.[6, 8] The global PES, although subject to some fitting errors through use of the EVB method, provides a good description of the dynamics of reaction of Cl atoms with propene. The extendable properties of the EVB formalism offer ready applications of the current work to both related alkene reactants and to liquid-phase simulations.

Acknowledgements

We thank EPSRC for funding through the Programme Grant EP/L005913/1. SP acknowledges the University of Bristol for the award of a postgraduate scholarship. We are grateful to David Tew and David Glowacki (University of Bristol) and Saulo Vázquez (Universidade de Santiago de Compostela) for valuable discussions.

Supporting Information Available

The Supporting Information contains a summary of structures and energies of intermediates and transition states obtained from the *ab initio* calculations, and further details of the EVB fits including the functional forms of the force fields, force-field parameter values, and coupling terms in the EVB matrices. It also shows plots of HCl(v=1, j) differential cross sections computed for different final rotational levels, and Boltzmann plots for rotational level populations obtained on all three EVB PESs. Velocity map images simulated using trajectory calculation outputs are compared with an experimental image. Examples are provided of animated trajectory files illustrating different types of reaction dynamics. This information is available free of charge via the internet at http://pubs.acs.org.

References

1. Wayne, R. P. *Chemistry of Atmospheres*. Third ed.; Oxford University Press: Oxford, 2000.
2. Arneth, A.; Schurgers, G.; Lathiere, J.; Duhl, T.; Beerling, D. J.; Hewitt, C. N.; Martin, M.; Guenther, A. Global Terrestrial Isoprene Emission Models: Sensitivity to Variability in Climate and Vegetation. *Atmos. Chem. Phys.* **2011,** *11*, 8037-8052.
3. Walavalkar, M.; Sharma, A.; Alwe, H. D.; Pushpa, K. K.; Dhanya, S.; Naik, P. D.; Bajaj, P. N. Cl Atom Initiated Oxidation of 1-Alkenes under Atmospheric Conditions. *Atmos. Environ.* **2013,** *67*, 93-100.
4. Shuman, N. S.; Stevens, W. R.; Lower, K.; Baer, T. Heat of Formation of the Allyl Ion by TPEPICO Spectroscopy. *J. Phys. Chem. A* **2009,** *113*, 10710-10716.
5. Cox, J. D.; Wagman, D. D.; Medvedev, V. A. Codata Key Values for Thermodynamics. Hemisphere Publishing Corp.: New York, 1989.
6. Preston, T. J.; Dunning, G. T.; Orr-Ewing, A. J.; Vazquez, S. A. Direct and Indirect Hydrogen Abstraction in Cl Plus Alkene Reactions. *J. Phys. Chem. A* **2014,** *118*, 5595-5607.
7. Brana, P.; Sordo, J. A. Theoretical Approach to the Mechanism of Reactions between Halogen Atoms and Unsaturated Hydrocarbons: The Cl Plus Propene Reaction. *J Comput Chem* **2003,** *24*, 2044-2062.
8. Pilgrim, J. S.; Taatjes, C. A. Infrared Absorption Probing of the $Cl+C_3H_6$ Reaction: Rate Coefficient for HCl Production between 290 and 800 K. *J. Phys. Chem. A* **1997,** *101*, 5776-5782.
9. Joalland, B.; Shi, Y.; Kamasah, A.; Suits, A. G.; Mebel, A. M. Roaming Dynamics in Radical Addition-Elimination Reactions. *Nature Comm.* **2014,** *5*, 4064.
10. Joalland, B.; Van Camp, R.; Shi, Y. Y.; Patel, N.; Suits, A. G. Crossed-Beam Slice Imaging of Cl Reaction Dynamics with Butene Isomers. *J. Phys. Chem. A* **2013,** *117*, 7589-7594.
11. Abou-Chahine, F.; Greaves, S. J.; Dunning, G. T.; Orr-Ewing, A. J.; Greetham, G. M.; Clark, I. P.; Towrie, M. Vibrationally Resolved Dynamics of the Reaction of Cl Atoms with 2,3-Dimethylbut-2-Ene in Chlorinated Solvents. *Chem Sci* **2013,** *4*, 226-237.
12. Chang, Y. T.; Miller, W. H. An Empirical Valence Bond Model for Constructing Global Potential-Energy Surfaces for Chemical-Reactions of Polyatomic Molecular-Systems. *J. Phys. Chem.* **1990,** *94*, 5884-5888.
13. Warshel, A.; Weiss, R. M. An Empirical Valence Bond Approach for Comparing Reactions in Solutions and in Enzymes. *J. Am. Chem. Soc.* **1980,** *102*, 6218-6226.
14. Glowacki, D. R.; Orr-Ewing, A. J.; Harvey, J. N. Product Energy Deposition of CN Plus Alkane H Abstraction Reactions in Gas and Solution Phases. *J. Chem. Phys.* **2011,** *134*, 214508.
15. Glowacki, D. R.; Rose, R. A.; Greaves, S. J.; Orr-Ewing, A. J.; Harvey, J. N. Ultrafast Energy Flow in the Wake of Solution-Phase Bimolecular Reactions. *Nature Chem.* **2011,** *3*, 850-855.
16. Dunning, G. T.; Glowacki, D. R.; Preston, T. J.; Greaves, S. J.; Greetham, G. M.; Clark, I. P.; Towrie, M.; Harvey, J. N.; Orr-Ewing, A. J. Vibrational Relaxation and Microsolvation of DF after F-Atom Reactions in Polar Solvents. *Science* **2015,** *347*, 530-533.
17. Glowacki, D. R.; Orr-Ewing, A. J.; Harvey, J. N. Non-Equilibrium Reaction and Relaxation Dynamics in a Strongly Interacting Explicit Solvent: $F + CD_3CN$ Modelled with a Parallel Multi-State EVB Model *J. Chem. Phys.* **2015**, *143*, 044120.
18. Hornung, B.; Harvey, J. N.; Preston, T. J.; Dunning, G. T.; Orr-Ewing, A. J. Empirical Valence Bond Theory Studies of the $CH_4 + Cl \rightarrow CH_3 + HCl$ Reaction. *J. Phys. Chem. A* **2015,** *submitted*.
19. Knizia, G.; Adler, T. B.; Werner, H. J. Simplified CCSD(T)-F12 Methods: Theory and Benchmarks. *J. Chem. Phys.* **2009,** *130*, 054104.
20. Peterson, K. A.; Adler, T. B.; Werner, H. J. Systematically Convergent Basis Sets for Explicitly Correlated Wavefunctions: The Atoms H, He, B-Ne, and Al-Ar. *J. Chem. Phys.* **2008,** *128*, 084102.
21. Werner, H. J.; Knowles, P. J.; Knizia, G.; Manby, F. R.; Schutz, M. Molpro: A General-Purpose Quantum Chemistry Program Package. *WIREs Comput. Mol. Sci.* **2012,** *2*, 242-253.

22. Schlegel, H. B.; Sonnenberg, J. L. Empirical Valence-Bond Models for Reactive Potential Energy Surfaces Using Distributed Gaussians. *J. Chem. Theory Comput.* **2006,** *2*, 905-911.
23. Hase, W. L.; Duchovic, R. J.; Hu, X.; Komornicki, A.; Lim, K. F.; Lu, D. H.; Peslherbe, G. H.; Swamy, S. R.; van de Linde, S. R.; Varandas, A., et al. Venus96: A General Chemical Dynamics Computer Program. *Quantum Chemistry Program Exchange (QCPE) Bulletin* **1996,** *16*, 671.
24. Lourderaj, U.; Sun, R.; Kohale, S. C.; Barnes, G. L.; de Jong, W. A.; Windus, T. L.; Hase, W. L. The Venus/NWChem Software Package. Tight Coupling between Chemical Dynamics Simulations and Electronic Structure Theory. *Comput. Phys. Commun.* **2014,** *185*, 1074-1080.
25. Murray, C.; Orr-Ewing, A. J. The Dynamics of Chlorine-Atom Reactions with Polyatomic Organic Molecules. *Int Rev Phys Chem* **2004,** *23*, 435-482.
26. Murray, C.; Pearce, J. K.; Rudic, S.; Retail, B.; Orr-Ewing, A. J. Stereodynamics of Chlorine Atom Reactions with Organic Molecules. *J. Phys. Chem. A* **2005,** *109*, 11093-11102.
27. Rose, R. A.; Greaves, S. J.; Orr-Ewing, A. J. Velocity Map Imaging the Dynamics of the Reactions of Cl Atoms with Neopentane and Tetramethylsilane. *J. Chem. Phys.* **2010,** *132*, 244312.
28. Rose, R. A.; Greaves, S. J.; Orr-Ewing, A. J. Velocity Map Imaging of the Dynamics of the CH_3 + HCl $\rightarrow$ CH_4 + Cl Reaction Using a Dual Molecular Beam Method. *Mol. Phys.* **2010,** *108*, 981-992.
29. Levine, R. D. *Molecular Reaction Dynamics*. Cambridge University Press: Cambridge, 2005.
30. Estillore, A. D.; Visger, L. M.; Suits, A. G. Imaging the Dynamics of Chlorine Atom Reactions with Alkenes. *J. Chem. Phys.* **2010,** *133*, 074306.

Table of Contents Graphic

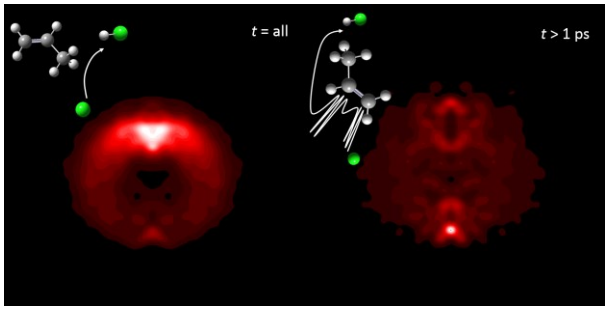

Possible Cover Artwork

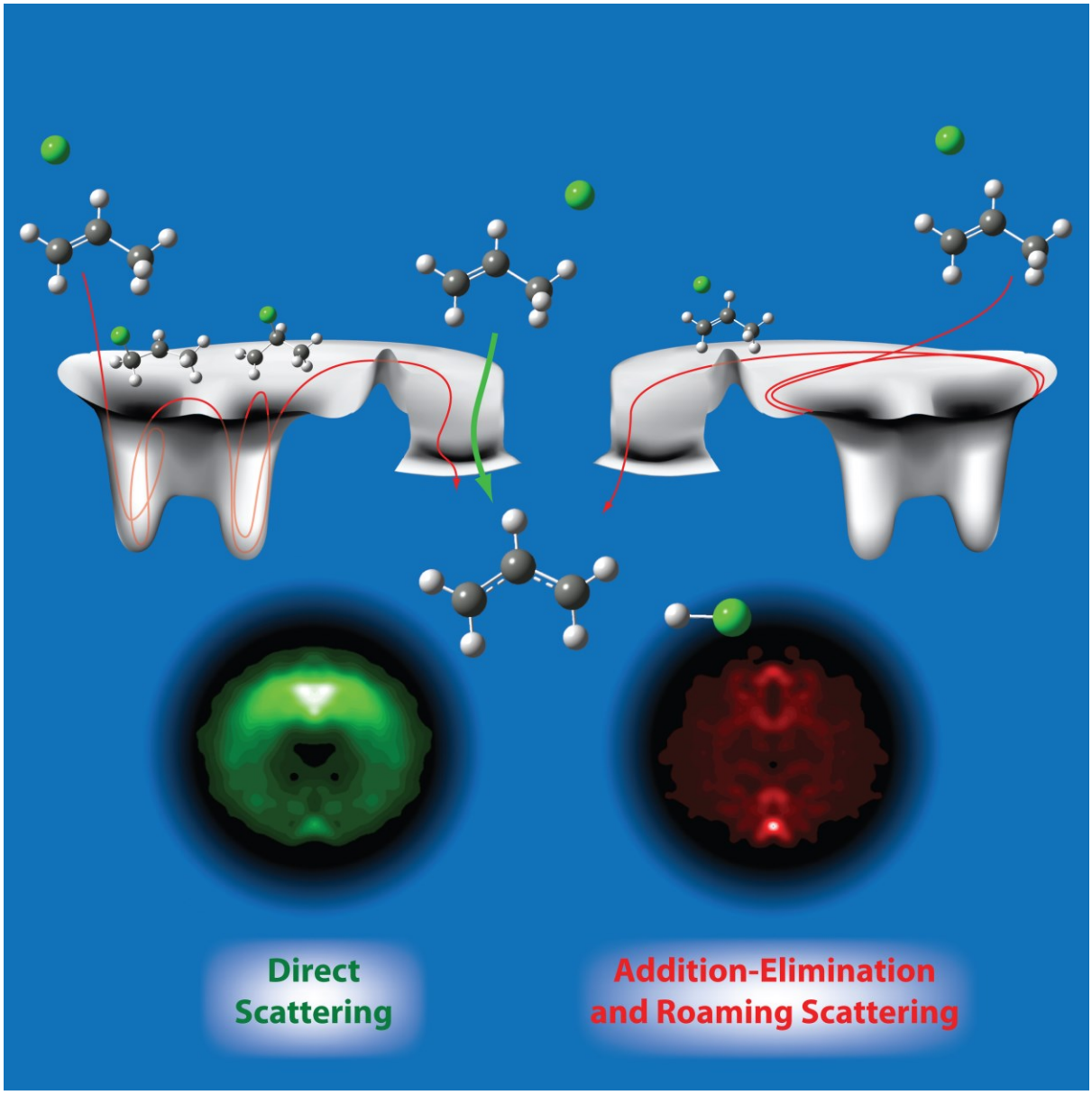

Direct, delayed and roaming pathways in the abstraction of a hydrogen atom from propene by a chlorine atom.